Supporting information

Selective shortening of gold nanorods: when surface functionalization dictates the reactivity of nanostructures

Abdelali Khelfa,[1] Jun Meng,[2.3.4] Caroline Byun,[1] Guillaume Wang,[1] Jaysen Nelayah,[1] Christian Ricolleau,[1] Hakim Amara,[1, 5] Hazar Guesmi,[2] Damien Alloyeau[1,]*

1. Laboratoire Matériaux et Phénomènes Quantiques, Université de Paris - CNRS, Paris, France

2. Institut Charles Gerhardt Montpellier, UM/CNRS/ENSCM, 34090 Montpellier, France

3. Division of Interfacial Water and Key Laboratory of Interfacial Physics and Technology, Shanghai Institute of Applied Physics, Chinese Academy of Sciences, Shanghai 201800, China

4. University of Chinese Academy of Sciences, Beijing 100049, China

5. Laboratoire d'Etudes des Microstructures, ONERA-CNRS, UMR 104, Université Paris Saclay, BP 72, 92322 Chatillon Cedex, France

Additional figures and details

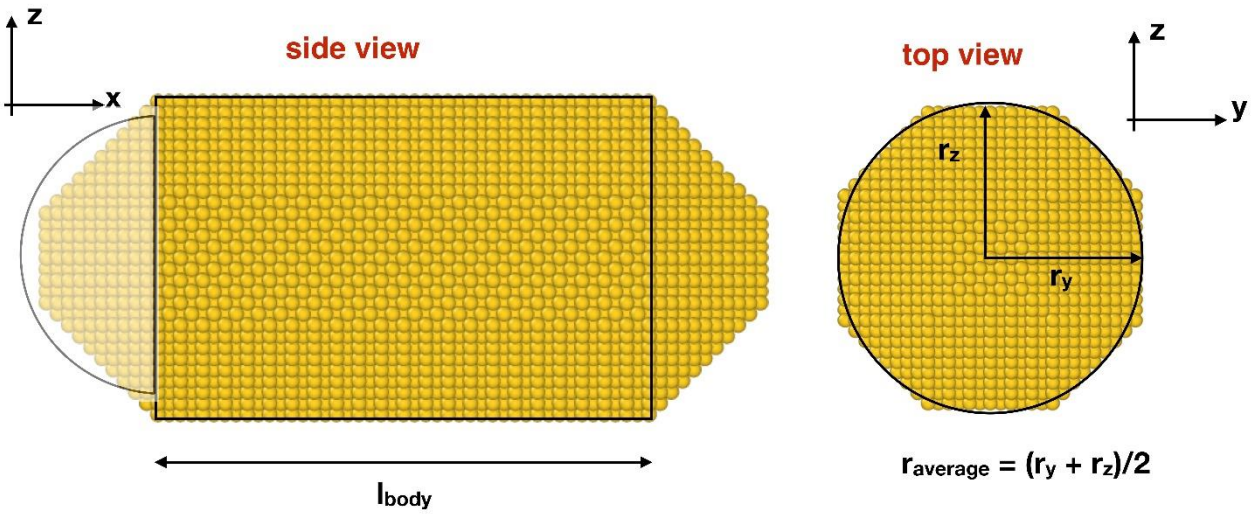

Figure S1. Approximation of the NRs by a cylinder and two half-spheres. The surface of the body and the tip is equal to $2\pi l_{body} \times r_{average}^2$ and $2\pi r_{average}^2$, respectively.

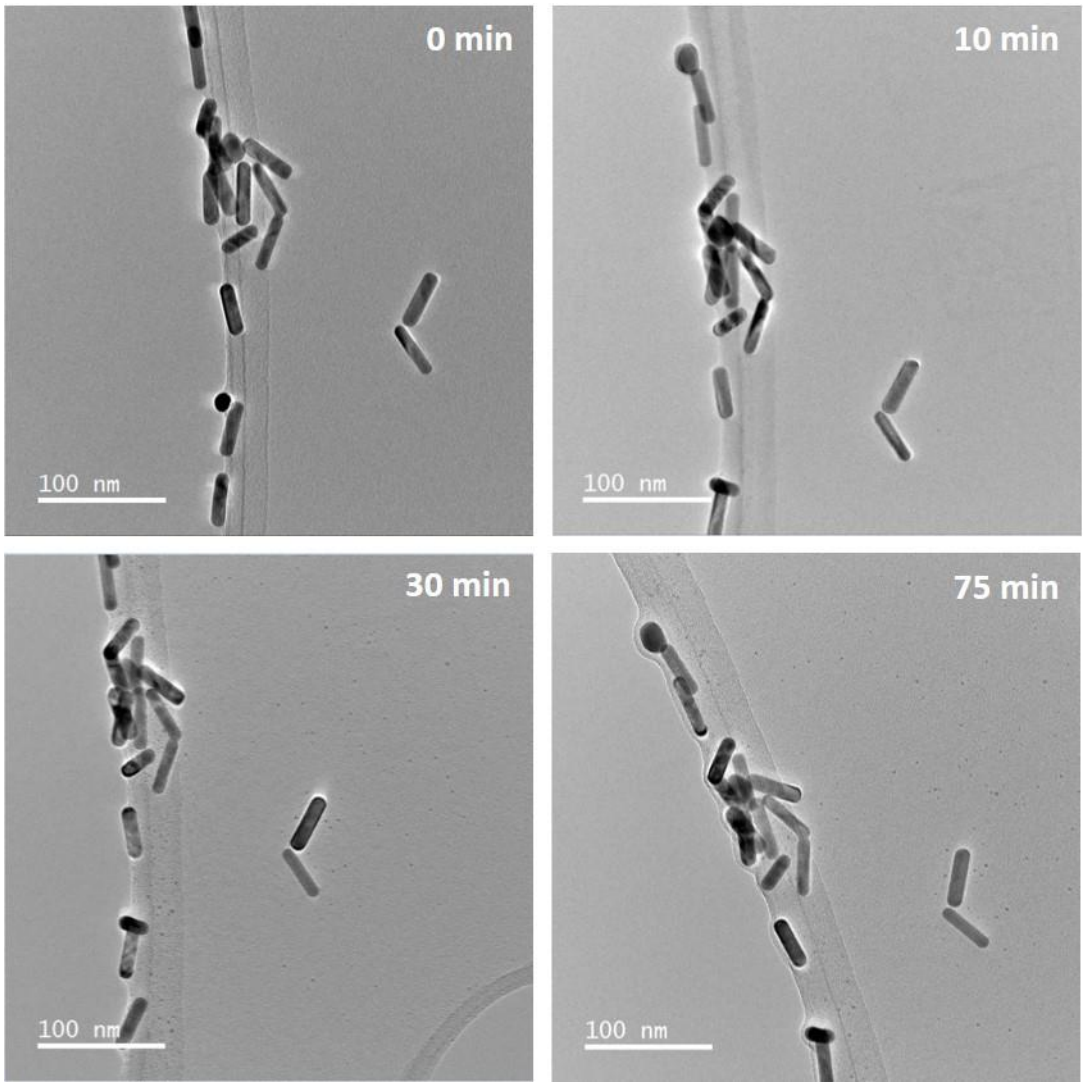

Figure S2. Ex situ control experiment (without electron beam). TEM image series showing the stability of NRs after an immersion time in the acidic saline solution (1M of NaCl and 10^{-2} M of HCl). After depositing the NRs on the carbon lacey TEM grid, the same area of the sample was imaged by TEM after each immersion step (the time indicated in the top-right corner of each image corresponds to the cumulative immersion time after each step). No degradation of the NRs was observed after 75 minutes in the solution revealing the key role of the electron beam in the etching processes observed by LCTEM.

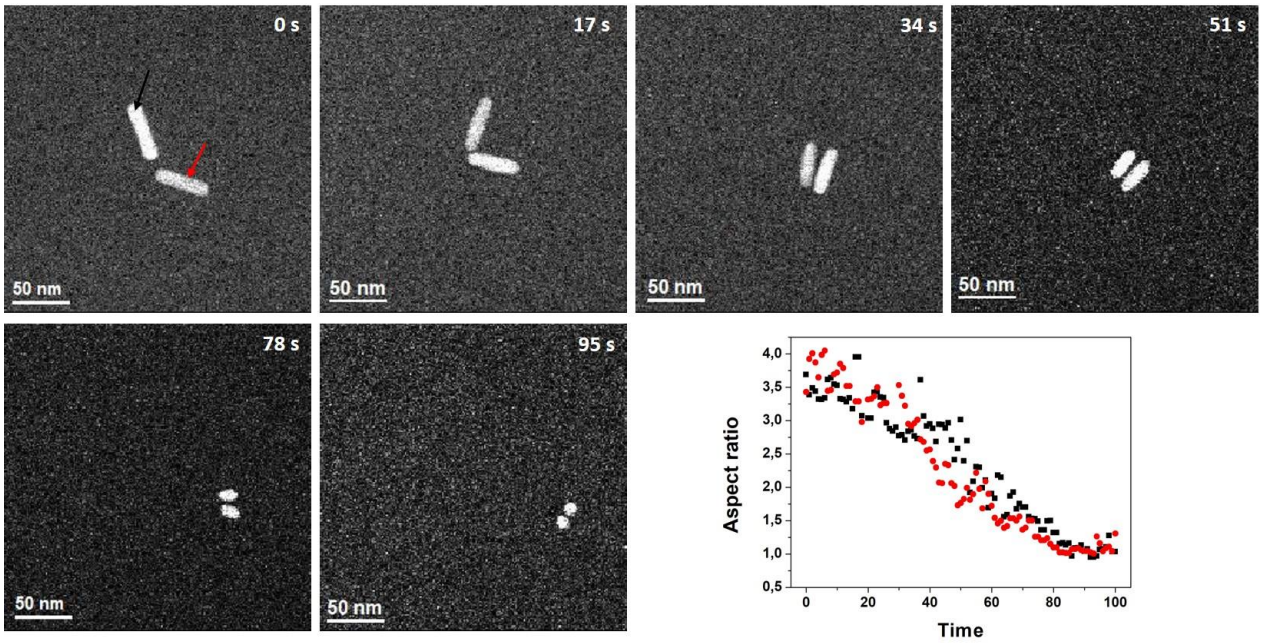

Figure S3. Selective shortening of gold NRs observed by LCTEM at low electron dose rate in the acidic saline solution. STEM HAADF image series acquired with an electron dose rate of 3.3 electron.s^{-1}.$Å^{-2}$. The acquisition time is indicated in the top right corner of each image. The time evolution of aspect ratio of the two observed NRs is seen in the botom right corner of the figure (the NRs corresponding to the black and red data points are indicated on the first image). See Video 3 in SI.

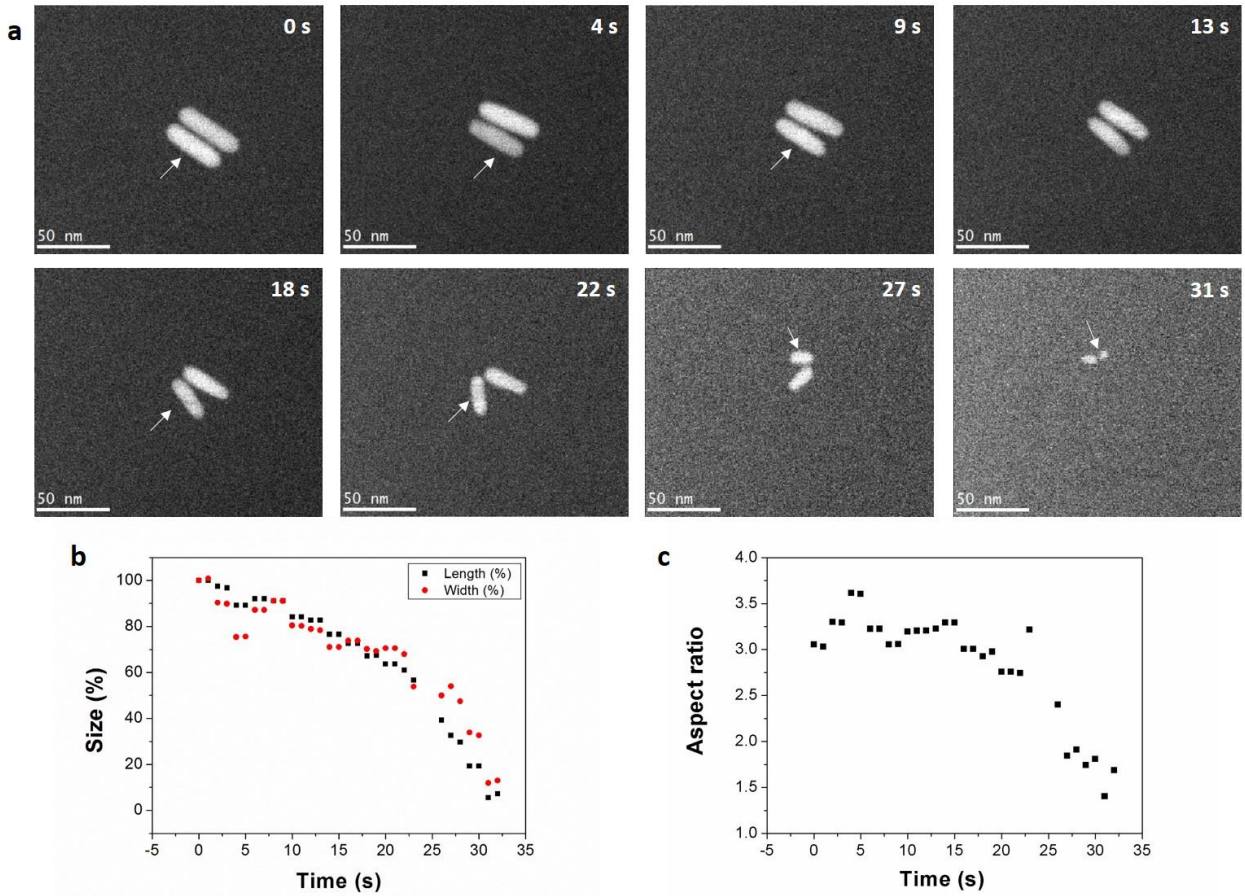

Figure S4. Isotropic etching observed by LCTEM at high electron dose rate in the acidic saline solution. (a) STEM HAADF image series acquired with an electron dose rate of 20.5 electron.s^{-1}.$Å^{-2}$. The acquisition time is indicated in the top right corner of each image. Time evolution of (b) the normalized length and width and (c) the aspect ratio of the NR indicated with an arrow in (a). See Video 2 in SI.

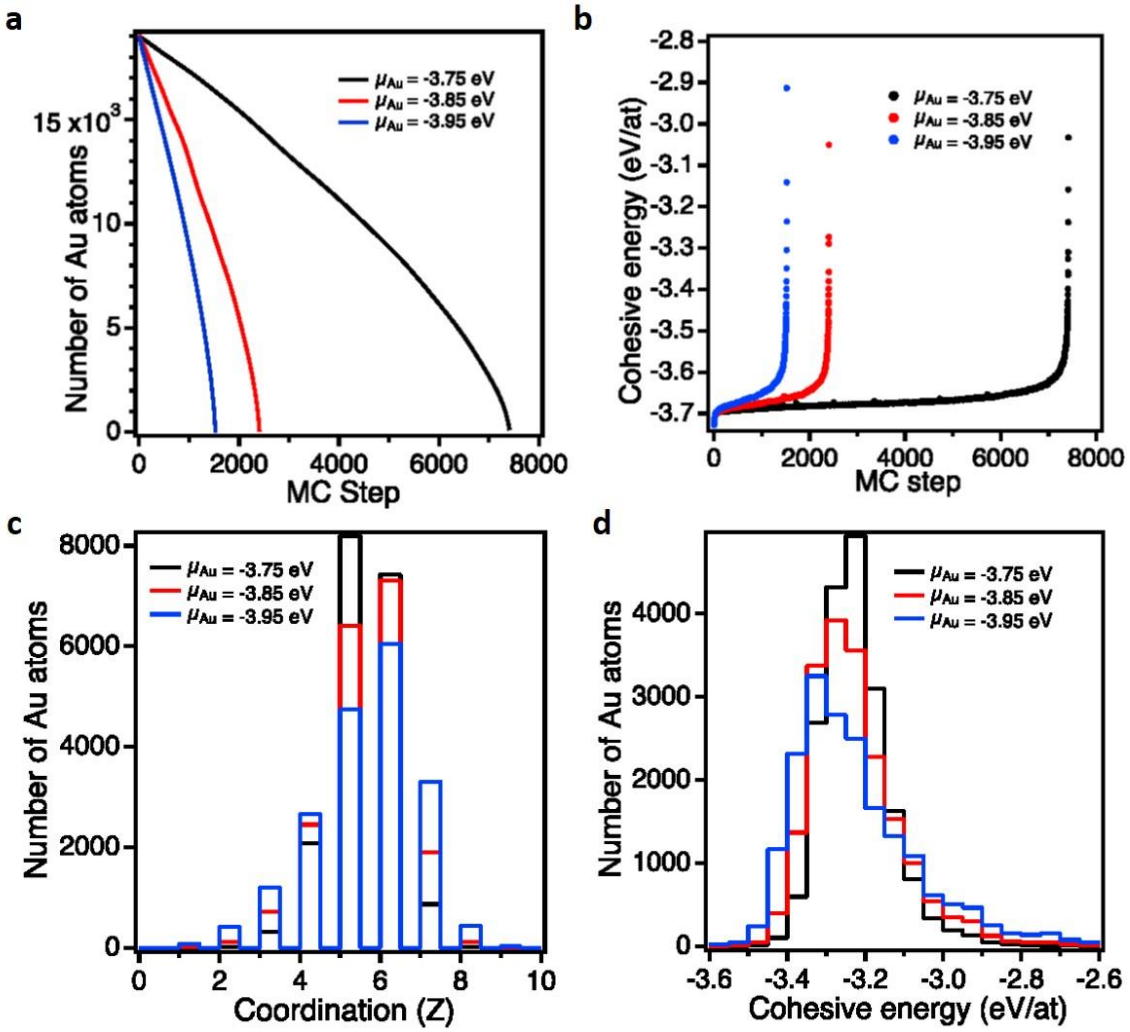

Figure S5. Grand Canonical Monte Carlo (GCMC) simulations of the dissolution of a citrate-free NR for three different chemical potentials. (a) Number of gold atoms in the NR as a function of MC step. (b) Cohesive energy per atom in the NR as a function of MC step (c) Coordination-number distribution of extracted atoms. (d) Desorption-energy distribution of extracted atoms.

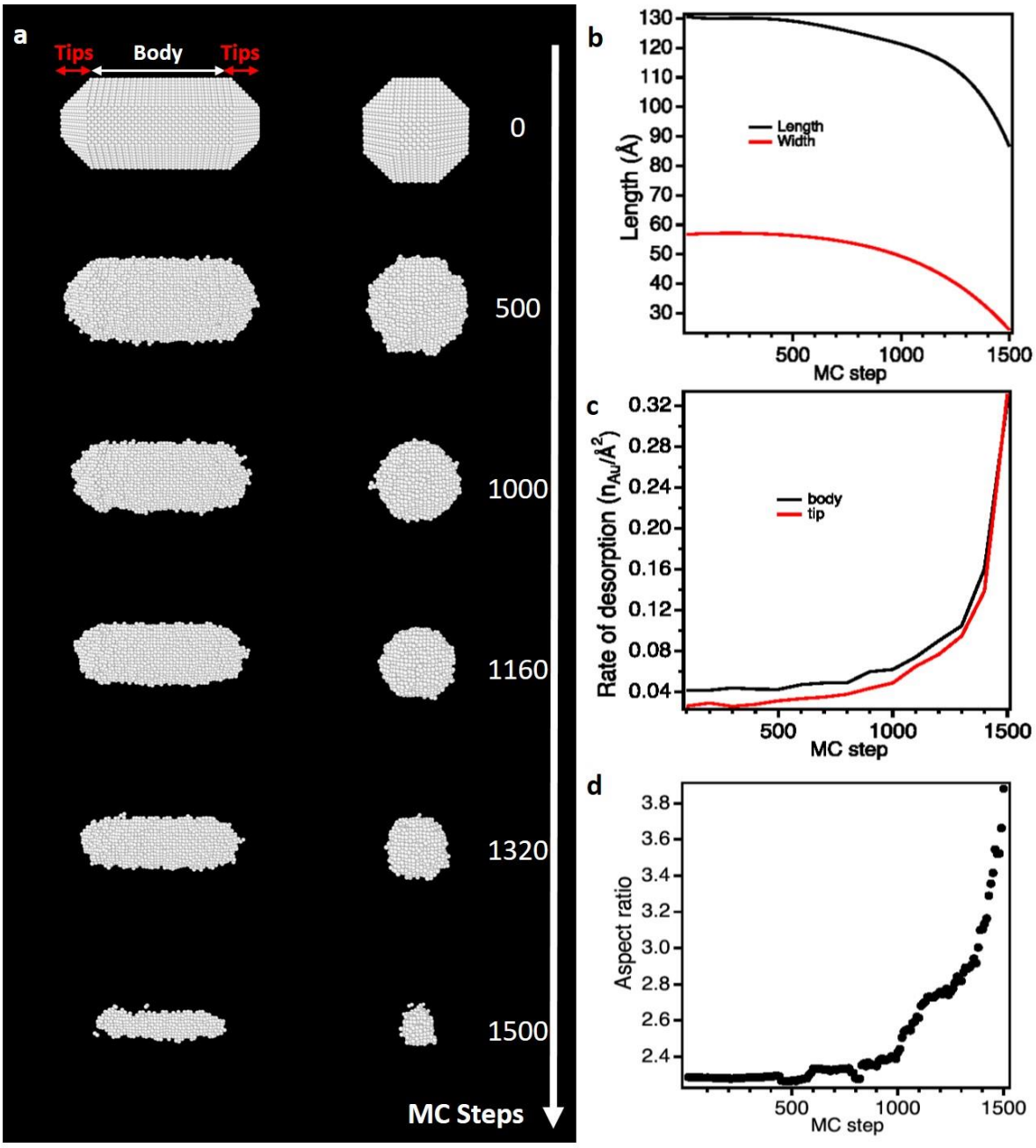

Figure S6. Monte Carlo (MC) simulations of the dissolution of a citrate-free NR using a strong chemical potential (μ_{Au} = -3.95 eV). (a) Snapshot images of the simulated NR seen along its transversal (left) and longitudinal (right) axes at different MC steps. (b) Length and width of the NR as function of MC step. (c) Rate of desorption of gold atoms on the tips and the body of the NR as function of MC step. (d) Aspect ratio of the NR as function of MC step (see video 5 in SI and the calculation details in the methods section).

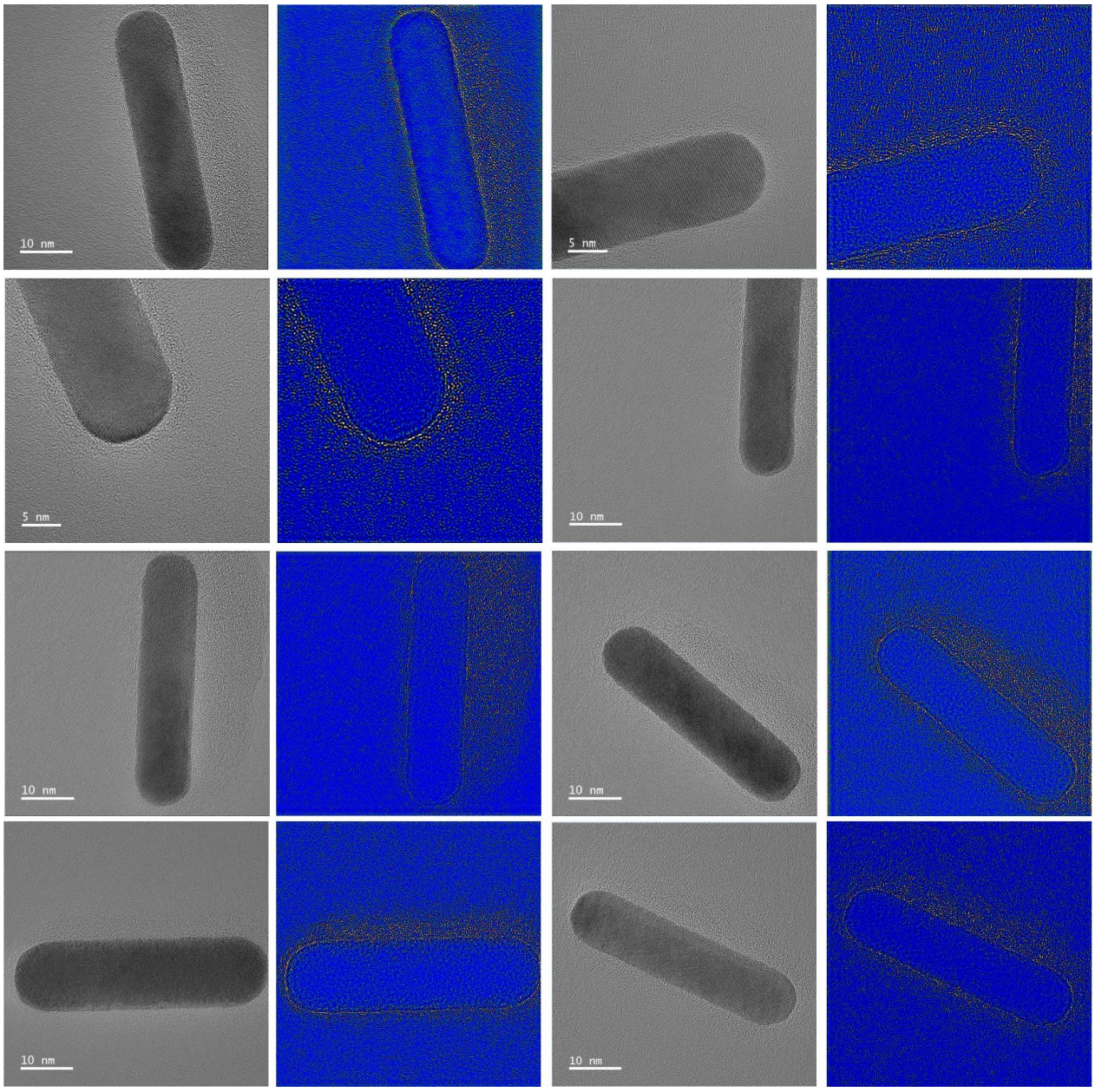

Figure S7. Spatial distribution of citrate functionalization over 8 gold NRs. On the left, original aberration-corrected HRTEM image acquired close to zero focus. On the right, same image on which we applied a low-pass filter and a color thresholding process to better visualize the citrate layer displayed in hot colors. Such images were used the measured the average thickness of the citrate layer on the body, the tips and the corners of NRs (see materials and methods).

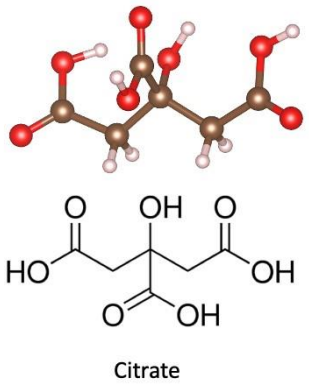

Figure S8. The optimized configurations and the structural formula of citrate in the gas phase.

To study the interactions of acetate and citrate with Au surfaces, we considered the dissociative adsorption via carboxylate O-H terminal where H atom was assumed to be dissociated in the solution and to diffuse onto the Au surface (see Fig. S9).

Figure S9: Illustration of the considered dissociative adsorption of the molecule. Au, C, O and H atoms are represented in yellow, black, red and white, respectively.

Detailed analysis of citrate adsorption

The computed adsorption configurations of citrate on Au surfaces through one terminal carboxylate group (C_2 configuration) are shown in Figure S10. Here as well, we have tested several possible adsorption sites to check the effects of the different surface sites. After optimizations, the results show that the most stable configuration is when the two oxygen atoms are combined to one Au surface atom and its first nearest neighbor Au atom (Table S1). Over the (110) surface, the configuration in which oxygen atoms of carboxylate group interact with two second Au atom neighbors is found to be less stable than the one engaging two Au first neighbors by about 0.08 eV.

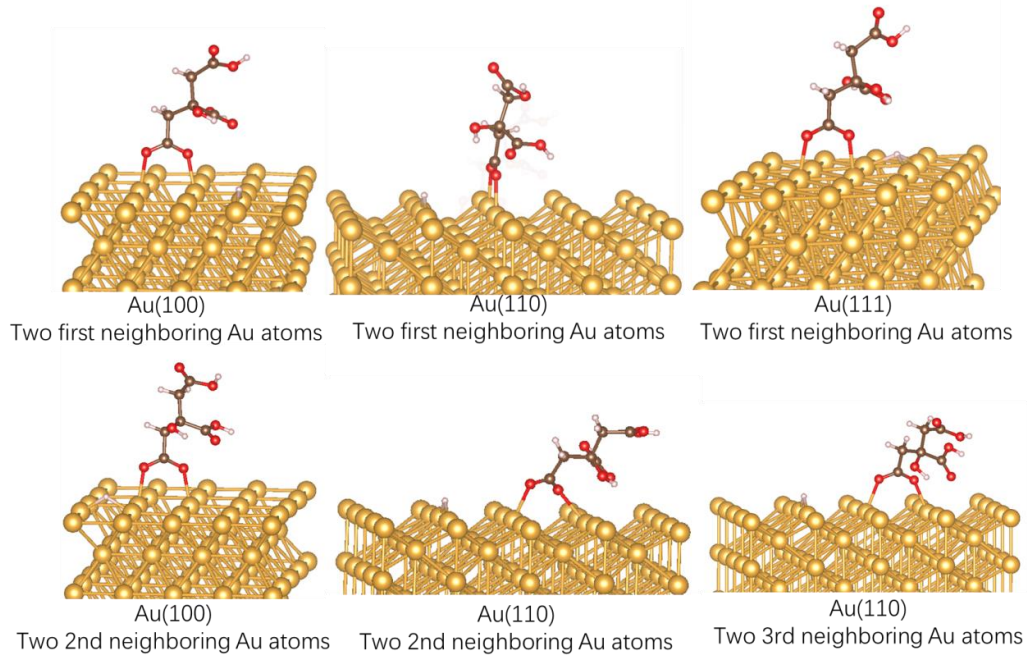

Figure S10. The optimized configuration of citrate on Au(100), Au(110) and Au(111) surfaces though one terminal carboxylate group.

Table S1. The adsorption energies of citrate on the Au surfaces through one terminal carboxylate group.

Au atoms	**Au(100)**	**Au(110)**	**Au(111)**
first neighbors	-0.21	-0.49	0.05
2nd neighbors	unstable	-0.41	
3rd neighbors		unstable	

In order to understand the superior reactivity of the Au(110) surface toward the citrate and to compare it to the Au(100) and the Au(111) surfaces (-0.49 eV Vs. -0.21 eV and 0.05 eV), we calculated the Bader charges and the charge transfers between the different surfaces and the molecule. The Figure S11, shows the calculated Bader charges of the carboxylate atoms connected to two Au first neighboring surface atoms for each surface and the corresponding charge density

difference represented by isosurfaces. The results show strong charge transfer from the surface to the citrate molecule adsorbed on Au(110). Interestingly, the surface charge depletion seems to arise from upper as well as from deeper surface atoms.

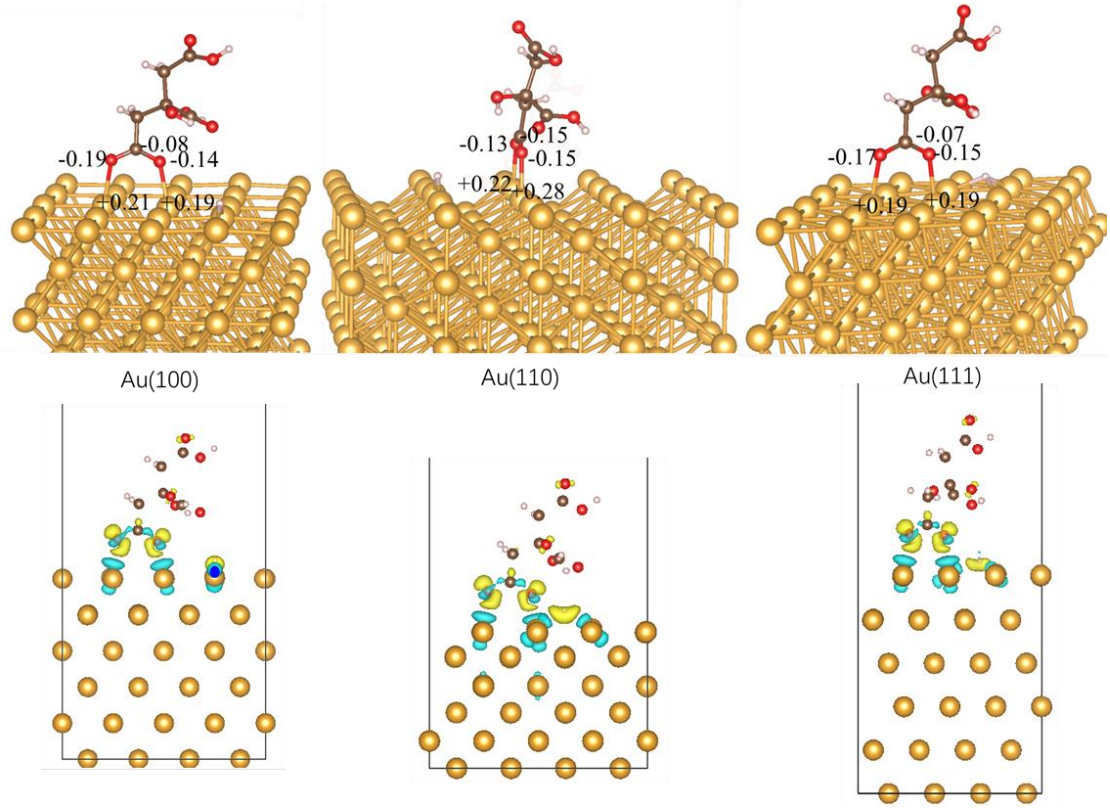

Figure S11. The Bader charges and the charge density difference of citrate adsorbed on the Au(100), Au(110), and Au(111) surfaces with the terminal COO^- group. The isosurface of the charge density is 0.005 e/Bohr^3.

The adsorption of citrate on high index surfaces (Au(221), Au(311) and Au(331))

As the tips of NRs present some surface defects (i.e. steps and small terraces) at the interface between (111), (110) and (100) faces, we investigated the adsorption of citrate on the Au(221), Au(311) and Au(331) surfaces that are shown in the Figure S12. The Au(311) surface can mimic the one-row missing step of the (111) surface. The Au(331) surface can represent the two-rows missing terrace of the (111) surface and one-row missing of the (110) surface. The (221) surface

can simulate the three-rows missing terrace of the (111) surface and three-rows missing terrace of the (110) surfaces. Although these high index surfaces were not identified experimentally, these three configurations could present different kinds of edge and terrace structures of the Au NRs.

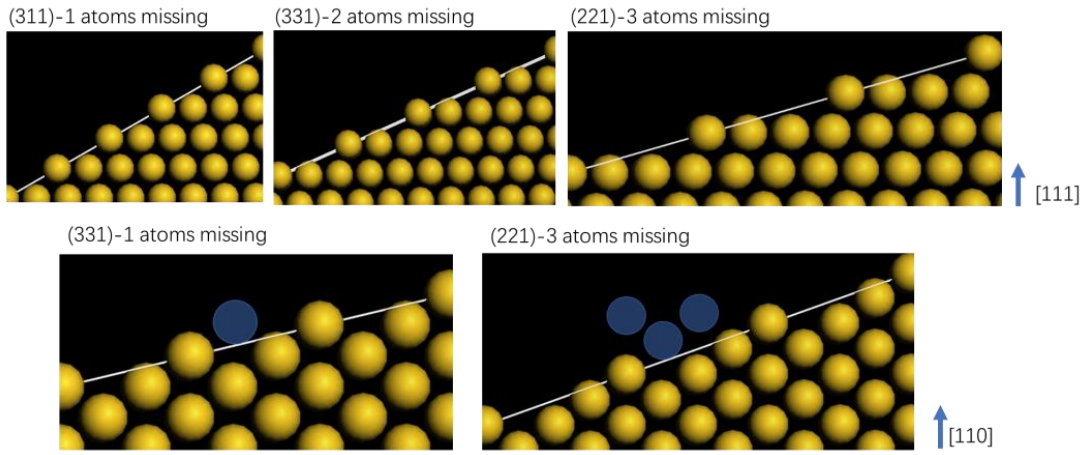

Figure S12. The surface structures of Au(221), Au(311), and Au(331) observed in cross section.

For each surface, different positions of the citrate bonding to the Au atoms are tested. The corresponding configurations which mostly correspond to C_2 conformations are summarized in Figure S13 and the adsorption energies are depicted in Table S2. In addition to the described configurations, we also studied the configurations of citrate bonded to the Au(221), (311) and the (331) facets through one terminal carboxylate and the central carboxylate (C4 conformation). However, the citrate became very unstable and messed up during the optimizations.

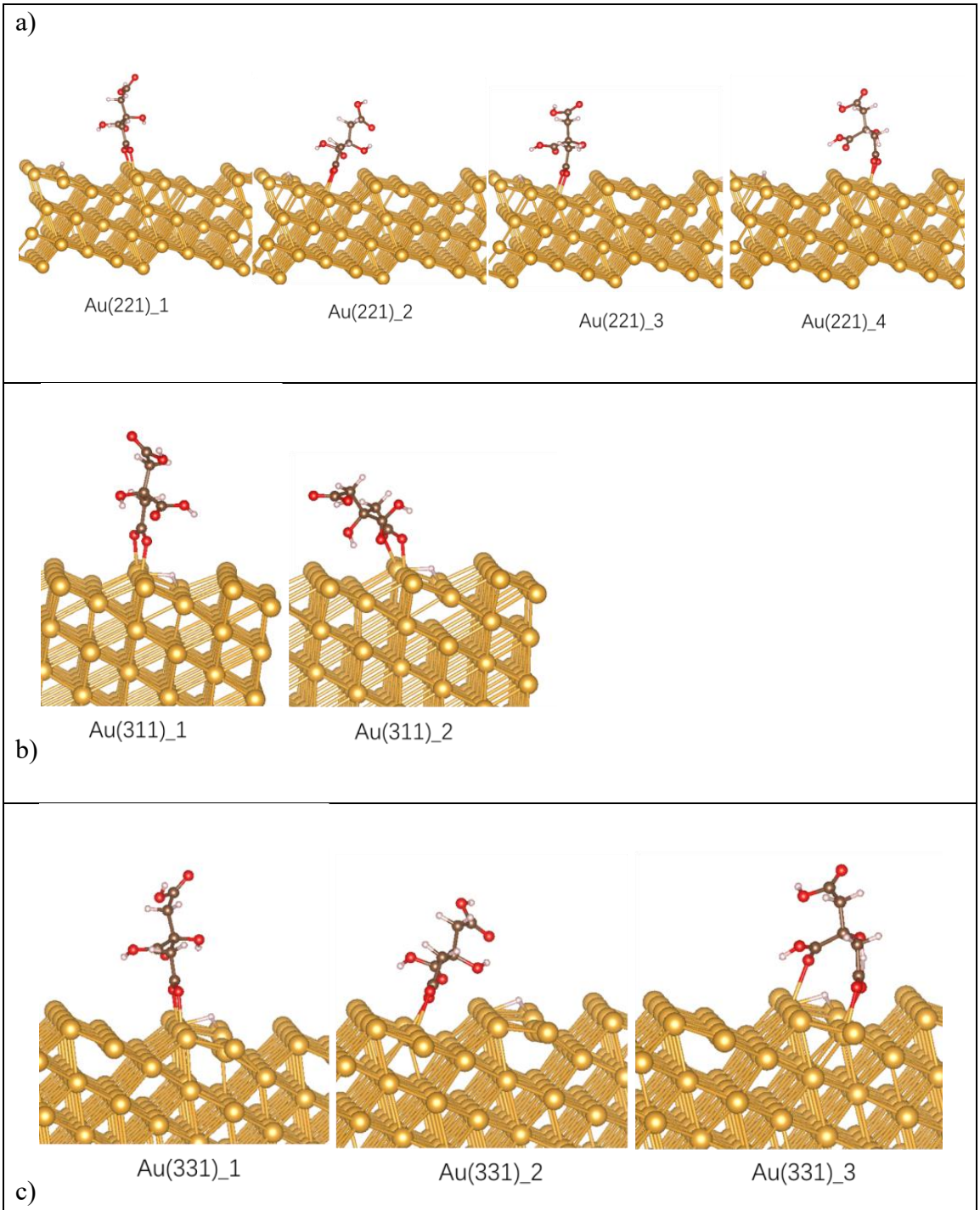

Figure S13. The optimized configurations of citrate on (a) Au(221) (b) Au(311) and (c) Au(331) surfaces though one terminal COO^- group.

Table S2. The adsorption energies of citrate on high index Au surfaces.

Citrate on Au(221) surface				
Configuration	1	2	3	4
E_{ad} (eV)	-0.17	-0.33	0.03	0.20
Citrate on Au(311) surface				
Configuration	1	2		
E_{ad} (eV)	-0.08	-0.31		
Citrate on Au(331) surface				
Configuration	1	2	3	
E_{ad} (eV)	-0.33	-0.43	-0.06	

It is worth noting that on these three high-index surfaces, step atoms at the edge of terraces are stable adsorption sites for citrate with competitive adsorption energies (E_{ad}<-0.3 eV). They are even the most stable sites on Au(221) and Au(311) surfaces. The DFT-D3 optimizations show the Au(331) to be the most reactive gold surface for citrate adsorption. Over this latter surface, the computed adsorption energies show two competitive adsorption sites (ΔE=0.1 eV), on the edge Au sites with E_{ad} predicted to be of -0.33 eV and over the Au terrace sites with E_{ad}=-0.43 eV. The adsorption energy of citrate on the Au(331) terrace sites is similar to the calculated adsorption energy on the (110) surface.

Associated Videos

There are 5 video files in SI:

Video 1 corresponds to the LCTEM data shown in figure 1a. It is accelerated 10 times with respect to raw data.

Video 2 corresponds to the LCTEM data shown in figure 1d and S4. It is accelerated 3 times with respect to raw data

Video 3 corresponds to the LCTEM data shown in figure S3. It is accelerated 10 times with respect to raw data

Video 4 corresponds to the GCMC Simulations shown in figure 3.

Video 5 corresponds to the GCMC Simulations shown in figure 3